



# Permeability modeling of Upper Cretaceous Bahariya Formation rocks, Abu Sennan field, Western Desert, Egypt

Hesham Hassan Abuseda<sup>1</sup> · Abdel Muktader Abdel Aziz El Sayed<sup>2</sup> · Osama Muhammad Elnaggar<sup>3</sup>

Received: 30 September 2022 / Accepted: 21 January 2023 / Published online: 1 March 2023  
© The Author(s) 2023

## Abstract

The present work aims to describe in detail the petrophysical properties of the Bahariya Formation (Abu Sennan field) through processing the core sample data and finding out the possible relations between permeability and other reservoir parameters such as porosity, specific internal surface, formation factor, and nuclear magnetic resonance to obtain reliable permeability prediction model of the Upper Cretaceous formation. The core samples have a length range of 2–4 cm with a diameter of 2.54 cm. Many petrophysical reservoir parameters were measured, such as permeability, porosity, density, formation factor, and special measurements such as spectral induced polarization, nuclear magnetic resonance, and specific internal surface. The samples cover a wide range of porosity (11.82–23.68 %) and permeability (0.06–133.65 mD). The porosity-permeability relationship indicates the increase of the permeability with porosity increase for the studied samples. The reservoir quality index ranges from 0.02 to 0.78  $\mu\text{m}$ . The flow zone indicator ranges from 0.09 to 3.39  $\mu\text{m}$  where pore throat radius ( $R_{35}$ ) ranges from 0.10 to 7.40  $\mu\text{m}$ . The reservoir quality index (RQI) and flow zone indicator (FZI) cross-plot show a better understanding of the formation evaluation. The hydraulic flow units are ( $0.09 \mu\text{m} < \text{FZI} \leq 3.39 \mu\text{m}$ ) and  $\text{RQI} < (1 \mu\text{m})$ . NMR longitudinal relaxation time  $T_1$  range is 1.21–175 ms, NMR transversal relaxation time  $T_{2(100)}$  range is 0.70–91.77 ms, and  $T_{2(600)}$  range is 0.74–75.86 ms. Models that incorporate porosity and NMR relaxation times will be more accurate and suitable for permeability prediction. Using multiple regression to determine the exponents of the power-law equation and replacing the porosity with the formation factor can improve the permeability prediction for the samples under investigation. The utilizing of NMR in predicting the permeability through a robust model considers an additional value for the Upper Cretaceous rocks in Egypt.

**Keywords** Permeability · Porosity · Specific internal surface · Spectral induced polarization · Nuclear magnetic resonance

## Introduction

Sandstone is a sedimentary rock (clastic type) composed of sand grains that originally were accumulated sediments subjected to diagenetic processes as cementation to join them into a rock. There are several types of sandstone. A rock is called sandstone if its components are mostly silicate. Different types of rocks are the host of the oil reserve all over the world, among them the sandstone reservoirs that should be porous and permeable. Sandstone petroleum reservoir mostly composed of quartz grains, rock fragments, feldspars, other minerals, and fluid (oil, water, gas) saturated spaces. Sandstone reservoirs mostly have porosity values ranges from 5 to 30% or more, while permeability ranges from 10 to 200 mD or more.

Most of the important hydrocarbon reservoirs in Egypt are in the Western Desert especially the Upper Cretaceous

---

Responsible Editor: Santanu Banerjee

✉ Osama Muhammad Elnaggar  
osama\_221@yahoo.com

Hesham Hassan Abuseda  
heshamabuseda@yahoo.com

Abdel Muktader Abdel Aziz El Sayed  
muktader76@yahoo.com

<sup>1</sup> Production Department, Egyptian Petroleum Research Institute (EPRI), Nasr City, Cairo 11727, Egypt

<sup>2</sup> Department of Geophysics, Faculty of Sciences, Ain Shams University, Cairo 11566, Egypt

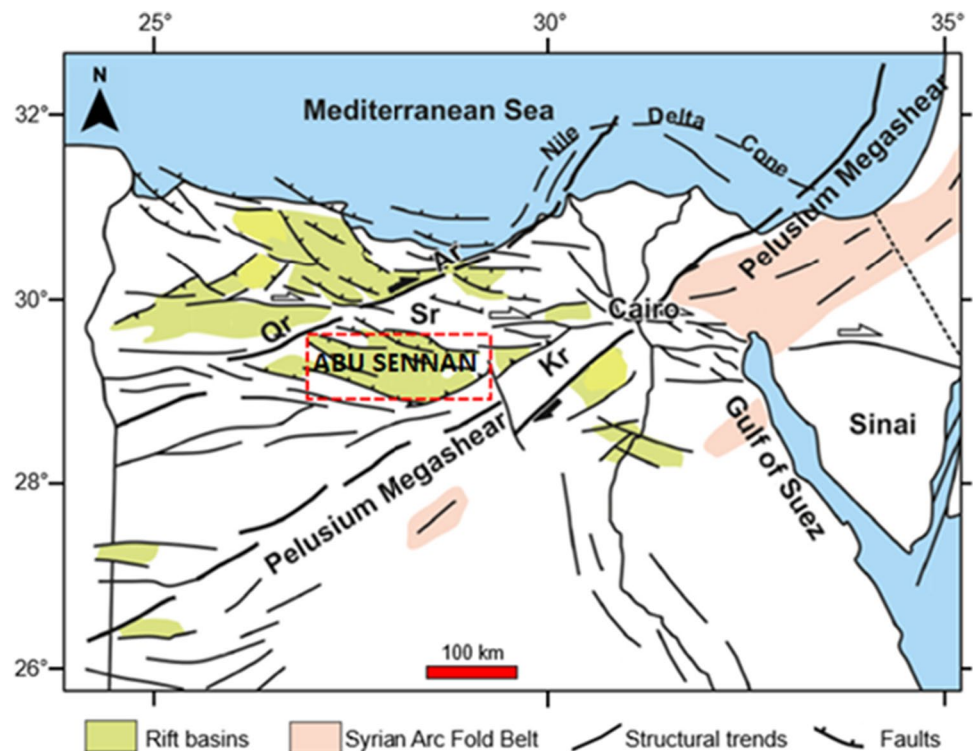
<sup>3</sup> Production Department, Egyptian Petroleum Research Institute (EPRI), Nasr City, Cairo 11727, Egypt

(Cenomanian) Bahariya Formation. Sandstone, limestone, shale, and siltstone are the main components of the Bahariya Formation. Several studies focused on the stratigraphy, tectonic, and sedimentology of the subsurface of the Bahariya Formation due to the importance of this formation in the hydrocarbon production (Soliman et al. 1970; El Gezeery et al. 1972; Franks 1982; Dominik 1985; Catuneanu et al. 2006; El Sayed et al. 1998; Matthias et al. 2009; El Sayed 2011; and El Sayed et al. 2019; Farouk et al. 2022 and Harishidayat et al. 2022). The Bahariya Formation was deposited in fluvio-marine to shallow marine conditions at the beginning of the Cenomanian transgression. The depositional environment experienced a coastal back stepping comprising coarsening upward cyclothems and the deposition of sandstones and siltstones and then a shallow marine with tidal flat to marine shelf environment settings. The Bahariya Formation is more or less conformably underlain by the Kharita Formation, where it is conformably overlain by the sandy limestone marker bed that constitutes the basal part of the Upper Cenomanian Abu Roash “G” Member. The Southwest Abu Sennan (SWS) field (the study area) that was located in the Abu Sennan concession is the main reservoir and the highest production in the Bahariya Formation. The location of the concession is between latitudes 29° 32' and 29° 49' N and longitudes 28° 35' and 28° 59' E in the Western Desert, 260 km west of Cairo and 160 km south of the Mediterranean coast. The concession approximately covers 3600 km<sup>2</sup> (Fig. 1).

The stratigraphic sequence of the (SWS) field is part of the North-Western Desert stratigraphic regime, which can be described in terms of the Upper Cretaceous and Tertiary Age. It is marked at many levels by unconformities of different magnitudes at the end of Kharita Formation, Abu Roash “E” Member, and also the end of Abu Roash “A” Member.

Concerning the present work, absolute permeability at the core scale is provided from laboratory measurements, which differ from the reservoir permeability. NMR is the valuable tool for estimating the in situ permeability (Hidajat et al. 2002 and Glover et al. 2006). The effect of the paramagnetic minerals such as iron oxide on the surface relaxivity can cause a shift in the relaxation distribution to a shorter times (Dodge et al. 1995). Previous studies proved a significant effect of the iron-bearing minerals on the permeability measurements using  $T_2$  NMR (Lala and El Sayed 2015). The aim of this study is to investigate the rock petrophysical characteristics, process the data from core samples, and then create a petrophysical model to predict permeability from nuclear magnetic resonance (NMR) data, focusing on the Upper Cretaceous Bahariya Formation in Abu Sennan field. The prediction of permeability is considered very important in the oil production and field development phases. The utilizing of NMR in predicting the permeability through a robust model considers an additional value for the Upper Cretaceous rocks in Egypt.

**Fig. 1** Location map of the study area, Abu Sennan field in the Western Desert along with the major structural features (Qr, Qattara Ridge; Sr, Sharib-Sheiba Ridge; Kr, Kattaniya Ridge). Adapted from Shalaby and Sarhan (2021)



## Methodology

### Sample preparation and techniques

All the samples of the Upper Cretaceous Bahariya Formation (Abu Sennan field) that were used in this study were cored using a diamond drilling machine; the sample length range is 2–4 cm and with a diameter of 2.54 cm. A solvent has been used to clean the studied samples, and then all the samples were dried in an oven to a constant weight at 105 °C to remove the remaining pore water and cleaning solvent. After the drying process, a petrophysical laboratory investigation was performed to estimate the petrophysical parameters for reservoir, such as density, permeability, porosity, formation factor, and special measurements such as spectral induced polarization, nuclear magnetic resonance, and specific internal surface. The porosity was measured using Core Lab's Helium Porosimeter; serial no. A-8222, model 3020-062, Dallas, TX, USA. The permeability was measured using Core Lab's Permeameter, the Mini Permeameter, model 302138, Dallas, TX, USA, and serial no. A-3148. The specific internal surface was measured using the nitrogen adsorption technique. The spectral induced polarization (SIP) was measured using the method mentioned in the "Spectral induced polarization" section. Relaxation measurements were performed with an NMR Rock Core Analyzer mentioned in the "Nuclear magnetic resonance" section.

### Porosity

The definition of reservoir rock porosity  $\Phi$  is the fraction of the reservoir bulk volume that is occupied with fluids to the solid framework of the reservoir (Tiab and Donaldson 2015). Mathematically, it can be expressed as Eq. (1):

$$\Phi = \frac{V_b - V_g}{V_b} = \frac{V_p}{V_b} \quad (1)$$

$\Phi$  is the porosity, frac. ;  $V_b$  is the bulk volume, cm<sup>3</sup>;  $V_g$  is the grain volume, cm<sup>3</sup>;  $V_p$  is volume of pore space, cm<sup>3</sup>.

Porosity controls the reservoir storage capacity which explains how important it is for determining the stored volume of reservoir fluids. Well logs and depositional environment interpretation were used for the prediction of reservoir evaluation (Al-Ghuribawi and Faisal 2021).

### Permeability

Rock permeability is the ability of a porous material to transmit fluid. Darcy's law describes permeability in porous media. Permeability depends on multiple parameters like cementation, pore geometry, texture of the rock, grain size,

and shape. Many studies investigated the porosity-permeability relationship (e.g., Carman 1937; Timur 1968; Scheiddegger 1974; Herron 1987; Adler et al. 1990; Schön 1996; Tiab and Donaldson 2015 and Lala and El Sayed 2017). Nitrogen gas permeameter was used to measure the permeability of the studied samples. The gas permeability ( $k$ ) is determined in a steady-state flow experiment using the pressure difference of upstream pressure ( $P_1$ ) and downstream pressure ( $P_2$ ) to calculate the flow rate  $q$  as shown in Eq. (2), the Darcy equation that relates the permeability to the compressible fluids.

$$k = \frac{\mu q L}{A (P_1^2 - P_2^2)} \quad (2)$$

$k$  is the permeability of the porous media, mD.  $\mu$  is the fluid viscosity, centipoises (cP).  $q$  is the flow rate cm<sup>3</sup>/s.  $L$  is the rock sample length, cm.  $A$  is the cross-sectional area of the rock, cm<sup>2</sup>.  $P_1$  and  $P_2$  are the inlet and outlet pressures, atm/cm.

### Flow unit

The reservoir heterogeneity and quality were determined using the hydraulic flow unit introduced by Amaefule et al. (1993), where  $RQI$  and  $FZI$  were defined as per Eqs. (3) and (4):

$$RQI = 0.0314 \sqrt{k/\Phi}, \quad (3)$$

$$FZI = \frac{RQI (1 - \Phi)}{\Phi}. \quad (4)$$

$RQI$  is the reservoir quality index,  $\mu\text{m}$ .  $K$  is the permeability, mD.  $\Phi$  is the porosity, frac.  $FZI$  is flow zone indicator,  $\mu\text{m}$ .

Estimated pore throat sizes ( $R_{35}$ ) from core-based porosity-permeability properties have been done.

### Specific internal surface

In the inhomogeneous and isotropic rocks, porosity is the available fraction of the rock for fluid flow. However, the individual pore sizes that control the fluid flow are not identified using porosity as an input data. Therefore, it is crucial to evaluate the average pore size and/or the pore throat size as input for permeability prediction models. We focus on using the surface area per unit pore volume ( $S_{\text{por}}$ , cm<sup>-1</sup>) to estimate the pore size. Based on a capillary bundle model, the  $S_{\text{por}}$  is inversely proportional to the pore radius ( $r$ ,  $\mu\text{m}$ ), where ( $A$ ) is the total surface of the sample in cm<sup>2</sup> and  $V_p$  is the pore volume.

$$S_{\text{por}} = \frac{A}{V_p} = \frac{2}{r} \quad (5)$$

Equation (6) shows that  $S_{\text{por}}$  can be calculated using the mass-related specific internal surface ( $S_m$ ) in  $\text{cm}^2/\text{g}$  when the porosity in (frac.) and the grain density ( $d_g$ ,  $\text{g}/\text{cm}^3$ ) of the material are known.

$$S_{\text{por}} = S_m d_g \frac{1 - \Phi}{\Phi} \quad (6)$$

Measuring the specific internal surface is done by using BET method through nitrogen gas adsorption technique (after Brunauer et al., 1938).

### Spectral induced polarization

The specific internal surface  $S_{\text{por}}$  also affects the spectral induced polarization (SIP). The rock induced polarization (IP) is affected by the electrical double layer (EDL) that forms along with the solid-liquid interface; this phenomenon has been thoroughly studied using theoretical and conceptual models where the polarization of the EDL surrounding a mineral grain and the polarization of pore throats were considered (e.g., Lesmes and Morgan 2001; Revil and Florsch 2010; Marshall and Madden 1959; and Titov et al. 2002). A linear relation between  $S_{\text{por}}$  and the electrical conductivity imaginary part and/or the normalized chargeability ( $m_n$ ) was identified by Weller et al. (2010b). The samples were saturated using 0.526 g/l ( $\sigma_w \approx 0.1$  S/m) sodium chloride solution (Abuseda et al. 2016). The saturated samples were installed in a core holder connected to two tanks with platinum current electrodes. The voltage was recorded by using the chlorinated silver wire rings that surround the sample as an electrode. All measurements were recorded in a climate controlled cabinet which also acts as a Faraday cage to reduce the influence of external electromagnetic noise. The temperature used was 20 °C. The error of the resistivity amplitude of the repeated SIP measurements is less than 3%, while the phase angles of complex resistivity determination error is less than 0.5 mrad.

### Nuclear magnetic resonance

Another estimation of  $S_{\text{por}}$  can be obtained using NMR. Coates et al. (1999) presented an excellent review of the NMR logging principles, while we only provide a brief fundamentals summary. Both the free pore fluid slow relaxation and pore surface's direct vicinity fast relaxation control the magnetic relaxation of excited hydrogen nuclei in a wetting pore fluid. If a fast diffusion exchange between the fluid at the pore surface and free pore fluid is present, a uniform pores' magnetization will exist, and the relaxation time will be proportional to the ratio of volume to surface. It is

important to determine the spectrum of different relaxation times in the case of varying pore size distributions which can be differentiated from the different types of relaxation times. The relation between the relaxation times and the surface to volume ratio which corresponds to the  $S_{\text{por}}$  (Kenyon, W.E., 1992) is expressed as follows:

$$\frac{1}{T_{1,2}} = \beta_{1,2} \frac{A}{V_p} \quad (7)$$

where  $T_{1,2}$  are NMR longitudinal and transversal relaxation times.  $\beta$  is the surface relaxivity.

In free fluids, no large difference is observed between  $T_1$  and  $T_2$ , because the relaxation time depends on the fluid viscosity. In natural rocks, the diffusion of the hydrogen nuclei in an inhomogeneous magnetic field generates dephasing effects that shorten  $T_2$  due to the susceptibility distribution. An NMR Rock Core Analyzer (Magritek) operating at a Larmor frequency of 2 MHz was used for the relaxation measurements at ambient pressure and temperature. We used a constant and short echo spacing of 600  $\mu\text{s}$  to eliminate the effect of diffusion. The sample axis was perpendicularly oriented with respect to the instrument's horizontal static magnetic field. The  $T_1$  and  $T_2$  relaxation times accuracy was in the order of 10%.

## Results and discussions

The samples cover a wide range of porosity (11.82–23.68%) with an average value of 18.25%, permeability (0.06–133.65 mD) with an average value of 51.02 mD, formation factor (12.45–62.40) with an average value of 26.23, specific internal surface (1.35–147.91  $1/\mu\text{m}$ ) with an average value of 40.33  $1/\mu\text{m}$ , and imaginary sigma (0.04–0.32 mS/m) with an average value of 0.15 mS/m. NMR longitudinal relaxation time  $T_1$  range is 1.21–175 ms with an average value of 60.19 s, NMR transversal relaxation time  $T_{2(100)}$  range is 0.70–91.77 ms with an average value of 35.99 s,  $T_{2(600)}$  range is 0.74–75.86 ms with an average value of 28.85 s, the reservoir quality index ranges from 0.02 to 0.78  $\mu\text{m}$  with an average value 0.39  $\mu\text{m}$ , flow zone indicator ranges from 0.09 to 3.39  $\mu\text{m}$  with an average value 1.52  $\mu\text{m}$ , and lastly pore throat radius ( $R_{35}$ ) ranges from 0.10 to 7.40  $\mu\text{m}$  with an average value 3.40  $\mu\text{m}$ .

### Petrophysical relationships

The main objective in this paper is to reveal the relationships between different petrophysical parameters and design a petrophysical model to estimate an important reservoir property that is difficult to be measured either in the laboratory or in the field.

**Porosity-bulk density**

An inverse relationship between bulk density and porosity is shown for Upper Cretaceous sandstone samples in Fig. 2. The following equation controls the relationship

$$\Phi = 0.68 - 0.23d_b \tag{8}$$

Coefficient of determination ( $R^2 = 0.87$ ).

where the bulk density  $d_b$  given in  $\text{g/cm}^3$  and the porosity  $\Phi$  as a fraction. The sandstone samples are characterized by high porosity and low density.

**Permeability-porosity**

In the present work, Fig. 3 shows the porosity-permeability cross-plot of the investigated samples. The data follows the expected positive trend between porosity and permeability. The relationship is characterized by a weak coefficient of determination of 0.42. The samples generally show lower porosity and permeability indicating that the samples are filled by clay minerals that cause a decrease in porosity and permeability (Abuseda and El Sayed 2022). The relation is controlled by the following equation:

$$k = [10]^{(27.54 \Phi - 4.36)} \tag{9}$$

**Reservoir quality index-porosity**

Figure 4 displays the relationship between the porosity and the reservoir quality index ( $RQI$ ) for all samples. The samples are characterized by  $RQI > 1 \mu\text{m}$ . These values indicate a fair to impervious reservoir quality. The porosity- $RQI$  relationship reads:

$$RQI = [10]^{(12.55\Phi - 3.09)} \tag{10}$$

It is characterized by a low coefficient of correlation ( $R^2 = 0.37$ ).

**Reservoir quality index-permeability**

Considering the definition of the  $RQI$  in Eq. (3), a strong correlation is expected between permeability and  $RQI$ . Figure 5 displays the nearly linear relationship between the permeability ( $k$ ) and the  $RQI$ . We got the following equation:

$$RQI = [10]^{(-1.13)} * [k]^{(0.48)} \tag{11}$$

It is characterized by a coefficient of correlation ( $R^2 = 0.997$ ). The reservoir quality index reflects mainly changes in permeability.

**Fig. 2** Porosity versus bulk density for Upper Cretaceous sandstone samples

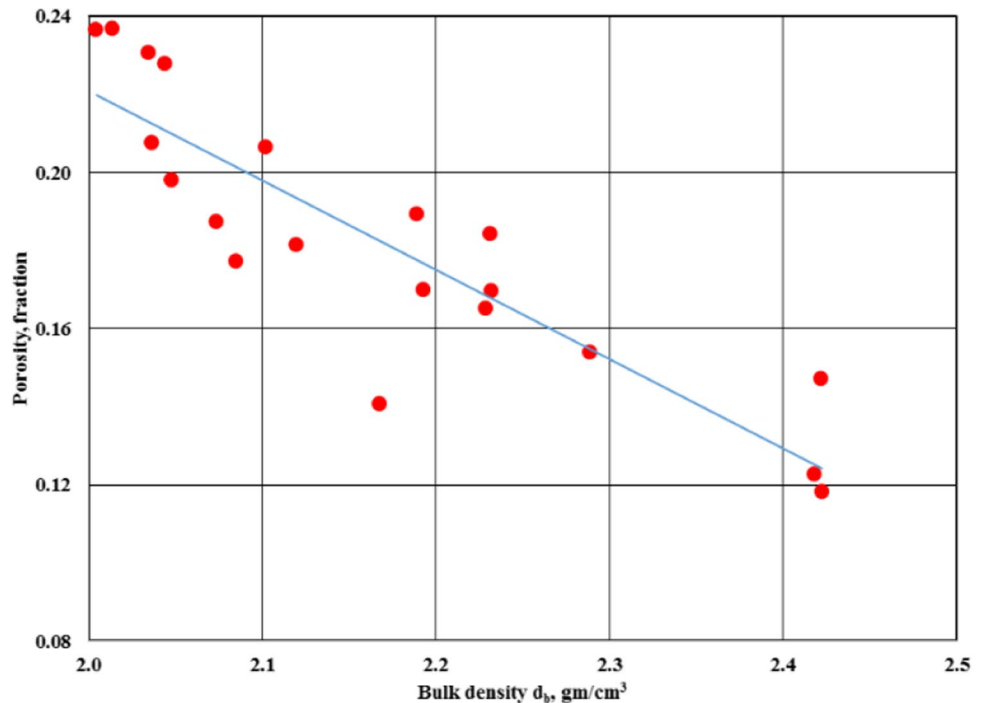


**Fig. 3** Permeability versus porosity for Upper Cretaceous sandstone samples

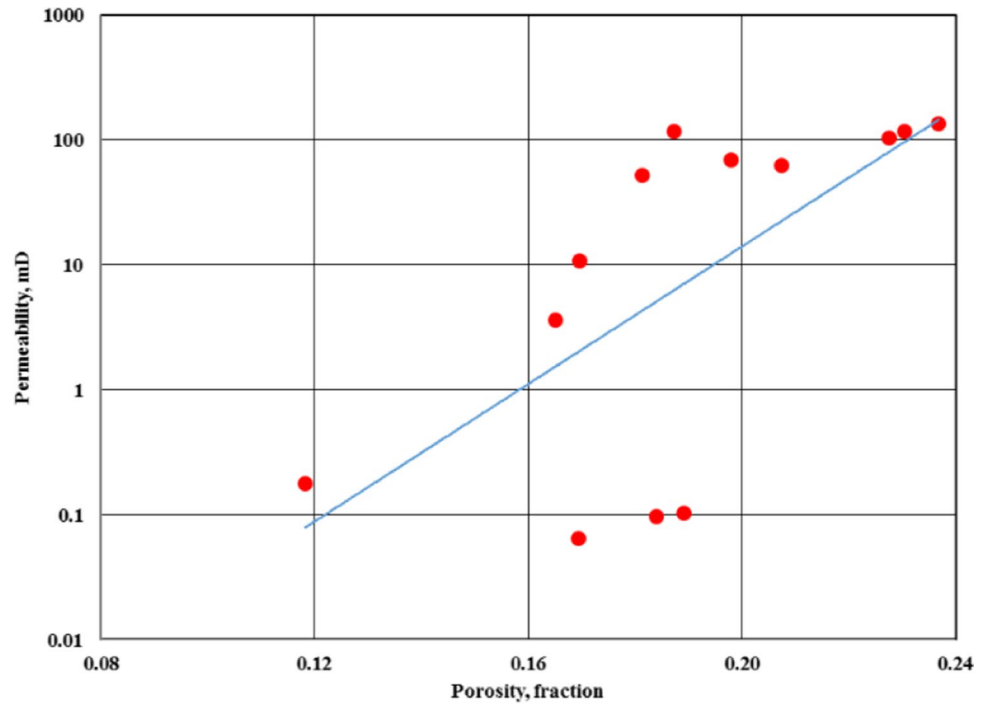
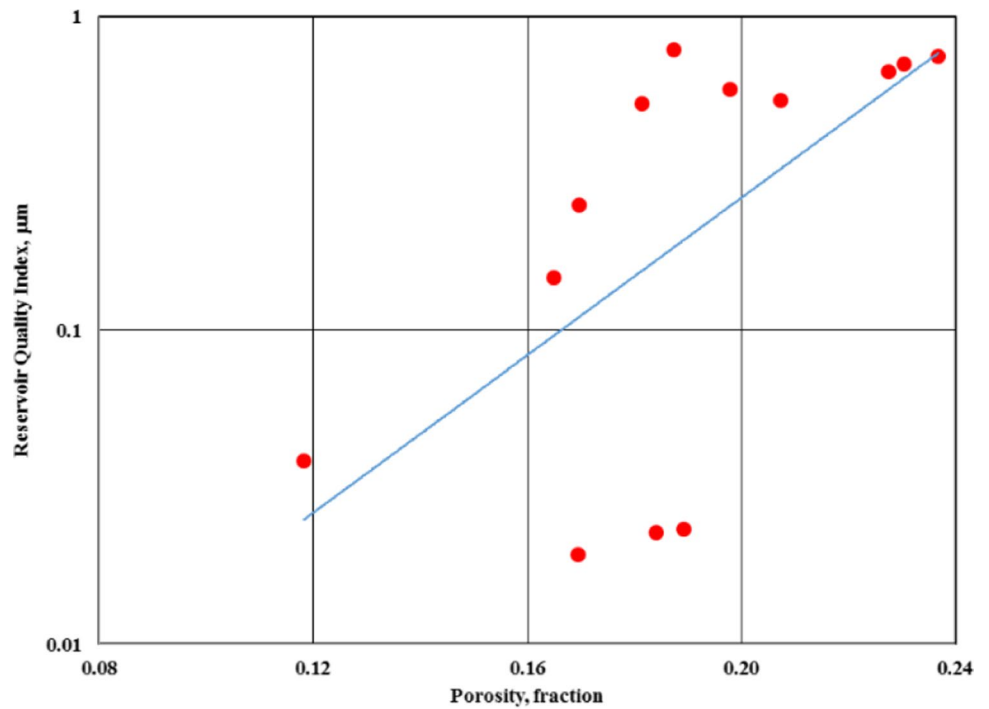


**Fig. 4** Reservoir quality index versus porosity for Upper Cretaceous sandstone samples

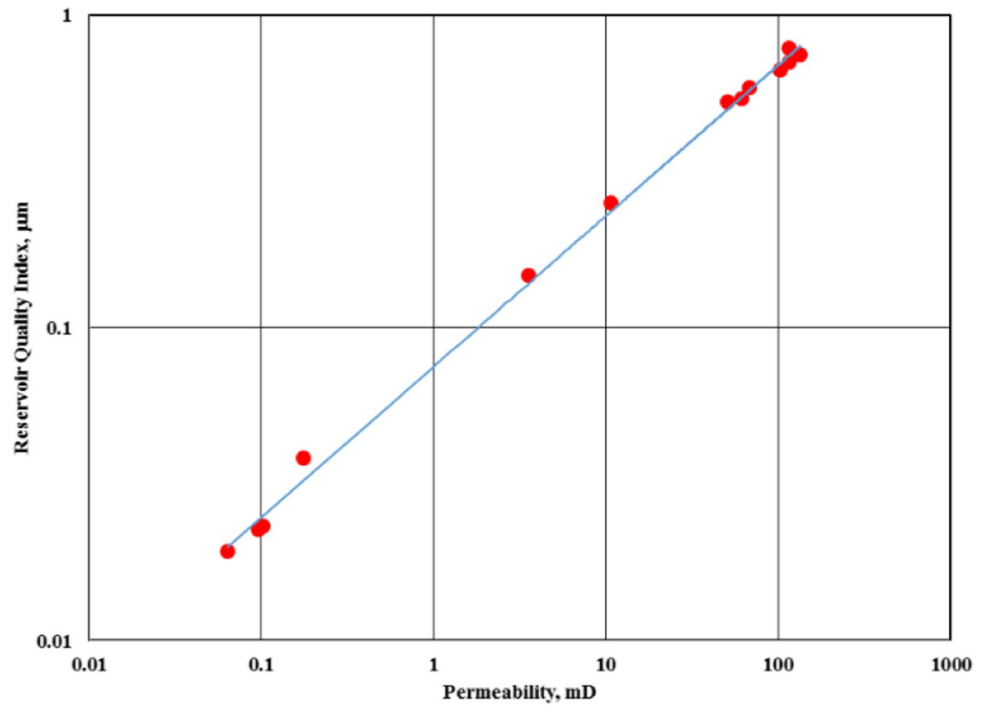


**Flow zone indicator-porosity**

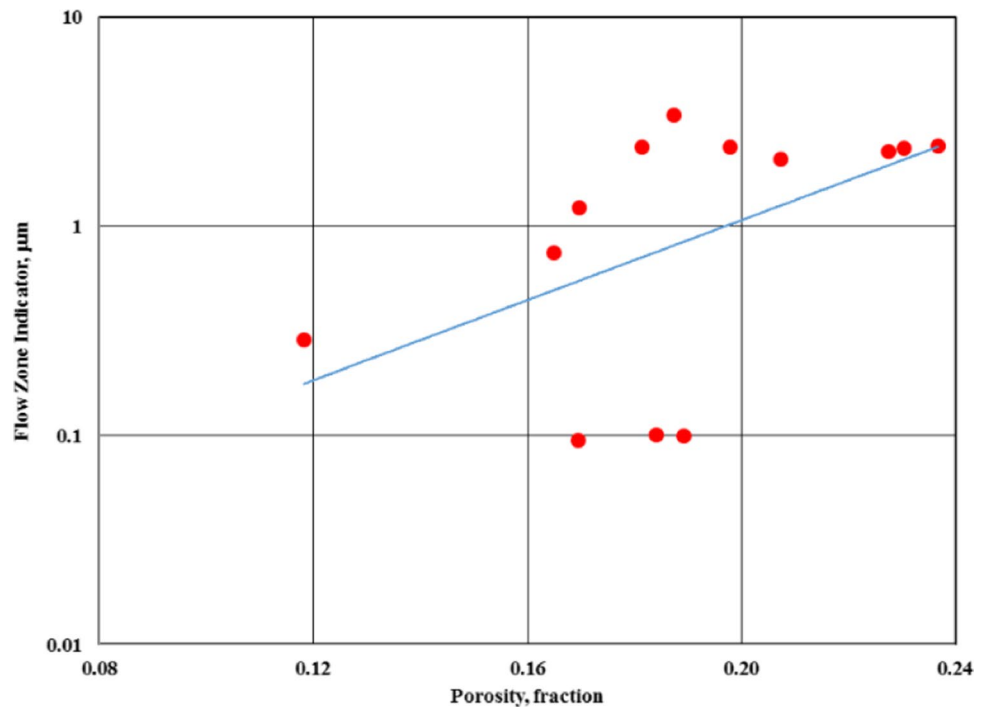
sandstone samples. Considering all data points, the graph

Figure 6 shows the relationship between the flow zone indicator and porosity for the studied Upper Cretaceous

**Fig. 5** Reservoir quality index versus permeability for Upper Cretaceous sandstone samples



**Fig. 6** Flow zone indicator versus porosity for Upper Cretaceous sandstone samples.

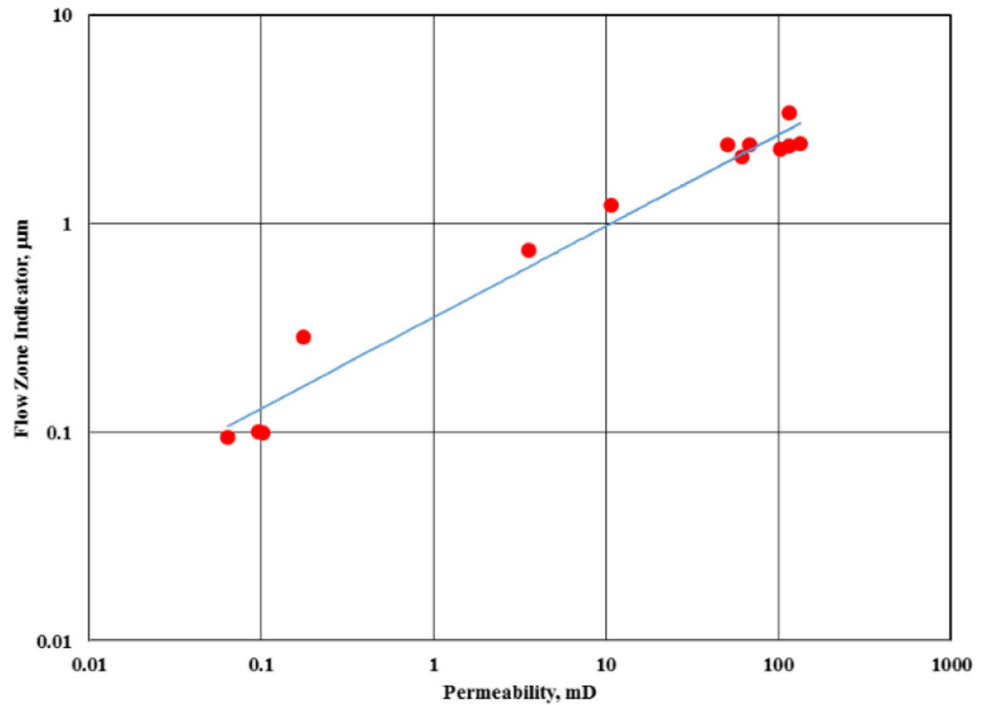


elucidates a weak relationship between *FZI* and porosity. The data points follow the expected positive trend between porosity and flow zone indicator for all investigated samples.

**Flow zone indicator-permeability**

Figure 7 shows the *FZI* as a function of the permeability for the studied rock samples, which are described by the following equation:

**Fig. 7** Flow zone indicator versus permeability for Upper Cretaceous sandstone samples



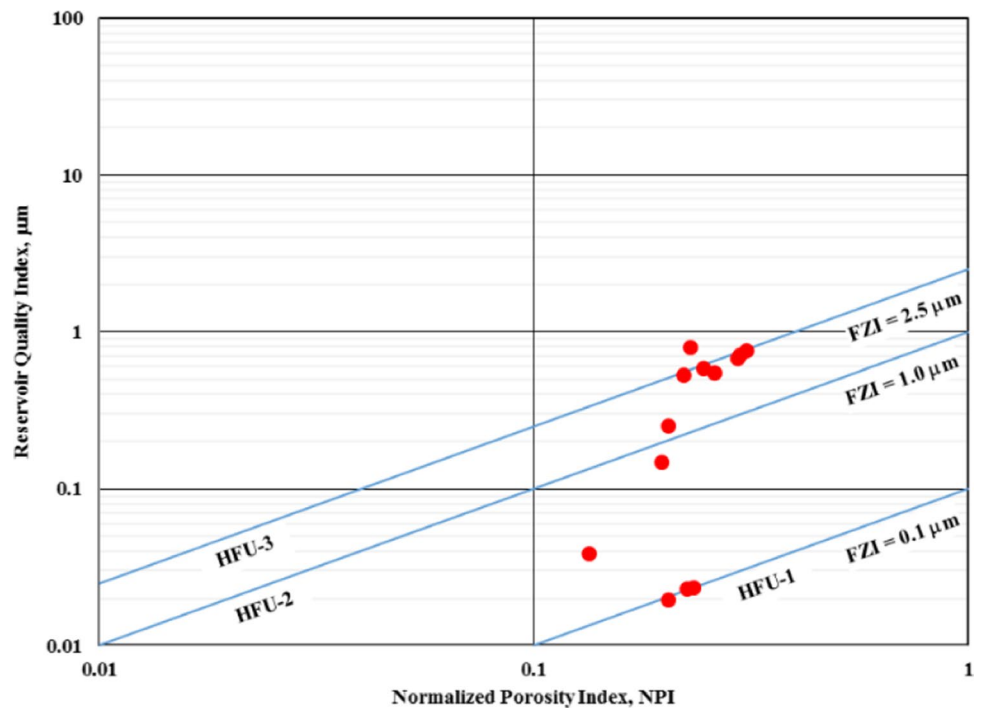
$$FZI = [10]^{(-0.45)} * [k]^{(0.44)}, \tag{12}$$

**Hydraulic flow units (HFUs)**

Considering the definition of *FZI* in Eq. (4), we found that the *FZI* depends mainly on permeability with a high coefficient of determination ( $R^2 = 0.97$ ).

Many authors used HFUs for permeability modeling and rock typing (e.g., Farouket al. 2021; Kassab and Taema 2018). The core analysis data were provided for the analysis of hydraulic flow units (HFU) (Amaefule et al. 1993). Equations (3) and (4), respectively, were used to calculate

**Fig. 8** Reservoir quality index versus normalized porosity index for Upper Cretaceous sandstone samples





*RQI* and *FZI* values. We plotted *RQI* as a function of *NPI* in Fig. 8 to characterize the flow properties, while three hydraulic flow units (HFU) are demarcated based on the *FZI* thresholds. The studied Upper Cretaceous samples are assigned to  $0.09 \mu\text{m} < \text{FZI} < 3.39 \mu\text{m}$ . Generally, rock pore systems containing clays in the form of filling, lining, and bridging as well as poorly sorted, fine-grained sands tend to display higher surface area and lower *FZI* values, whereas coarse-grained, well-sorted, and clean sands show lower surface areas and higher *FZI* values. A cross-plot between *RQI* and *FZI* provides a better understanding of the formation evaluation. Figure 9 displays that  $0.02 \mu\text{m} < \text{RQI} \leq 0.78 \mu\text{m}$  and refers to impervious to fair reservoir quality. We empirically derived the pore throat radius ( $R_{35}$ ) as a function of core-porosity and permeability using the Kolodzie model (1980). Estimated ( $R_{35}$ ) ranges from 0.10 to 7.40  $\mu\text{m}$  and is plotted against *RQI* and *FZI* (Fig. 10 A and B). The Upper Cretaceous sandstone sample reservoir is comprised of meso-microporosity ( $0.10 \mu\text{m} < R_{35} \leq 2 \mu\text{m}$ ) and macroporosity ( $2 \mu\text{m} < R_{35} \leq 10 \mu\text{m}$ ). Based on core-based reservoir characterization, we summarize that the macro-porosity of the Upper Cretaceous sandstone have the fair reservoir quality and hydraulic flow units ( $0.09 \mu\text{m} < \text{FZI} \leq 3.39 \mu\text{m}$ );  $\text{RQI} < (1 \mu\text{m})$ .

**Formation factor-porosity**

The cross plot between the log values of the formation factor and porosity is shown (Fig. 11). The data points follow

the expected trend with a decrease of formation factor with increasing porosity. The fitting equation is

$$F = \frac{1}{\phi^{1.85}} \tag{13}$$

where *F* is the formation factor, with a cementation factor  $m = 1.85$  results in a high coefficient of determination ( $R^2 = 0.70$ ).

**Permeability-formation factor**

The relation between permeability and formation factor is displayed (Fig. 12). Large formation factor values indicate lower porosity samples. The relationship is characterized by the determination coefficient  $R^2 = 0.68$  which is considerably higher than that of Eq. (9) and controlled by the following equation:

$$k = [10]^{8.46} * [F]^{-5.62} \tag{14}$$

**Permeability-internal surface ( $S_{por}$ )**

The specific internal surface ( $S_{por}$ ) and pore radius are related according to Eq. (5) and also controls permeability beside the porosity. Figure 13 shows the correlation between the permeability and internal surface, where coefficient of determination  $R^2 = 0.73$  and the fitting equation reads:

**Fig. 9** Reservoir quality index versus flow zone indicator for Upper Cretaceous sandstone samples

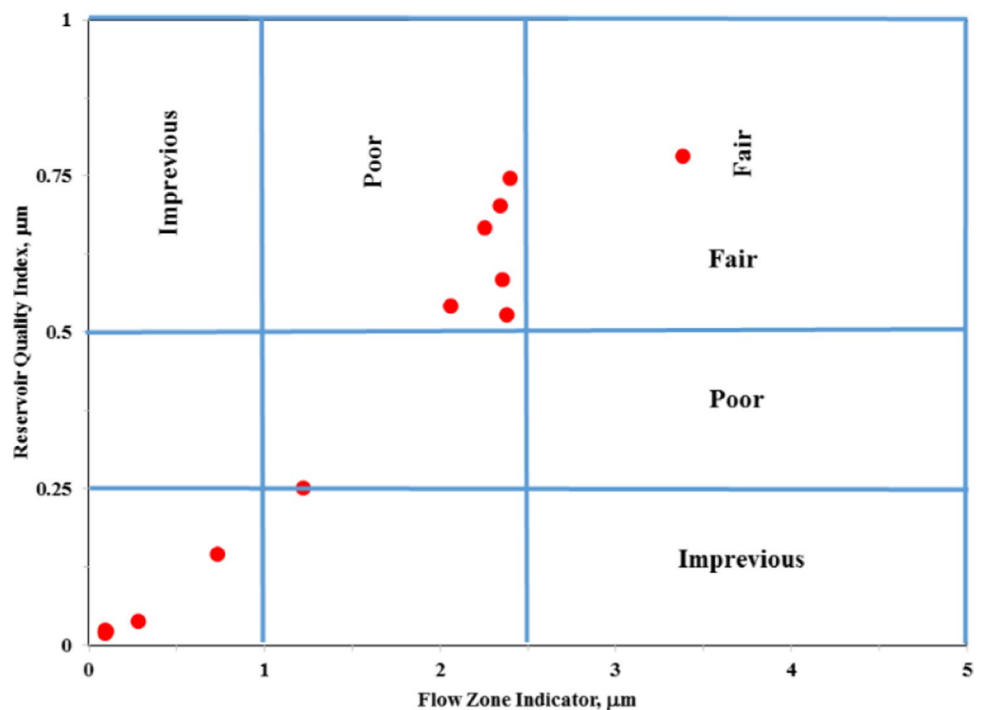
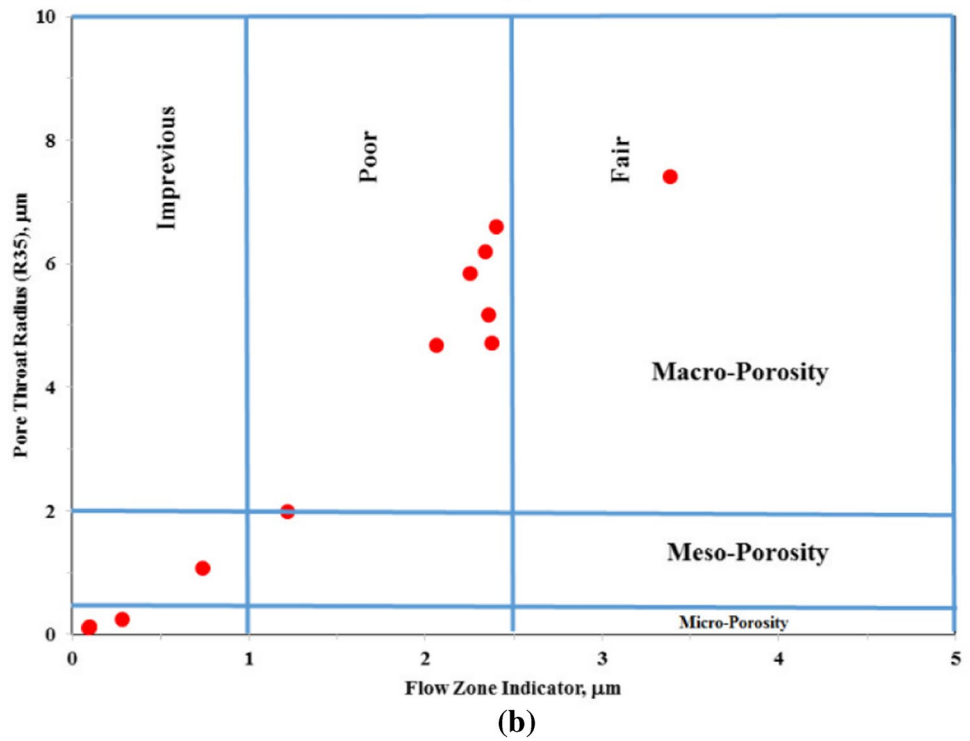
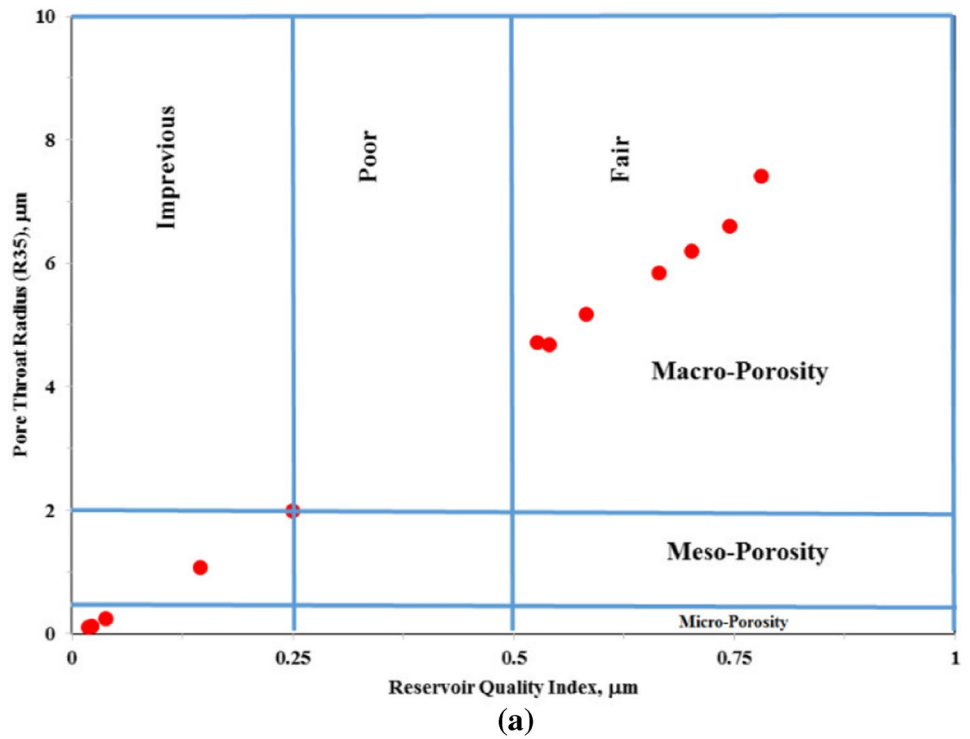


**Fig. 10** **A** Pore throat radius ( $R_{35}$ ) versus reservoir quality index for Upper Cretaceous sandstone samples. **B** Pore throat radius ( $R_{35}$ ) versus flow zone indicator for Upper Cretaceous sandstone samples



$$k = [10]^{2.69} * S_{\text{por}}^{-1.76} \tag{15}$$

**Fig. 11** Formation resistivity factor versus porosity for Upper Cretaceous sandstone samples

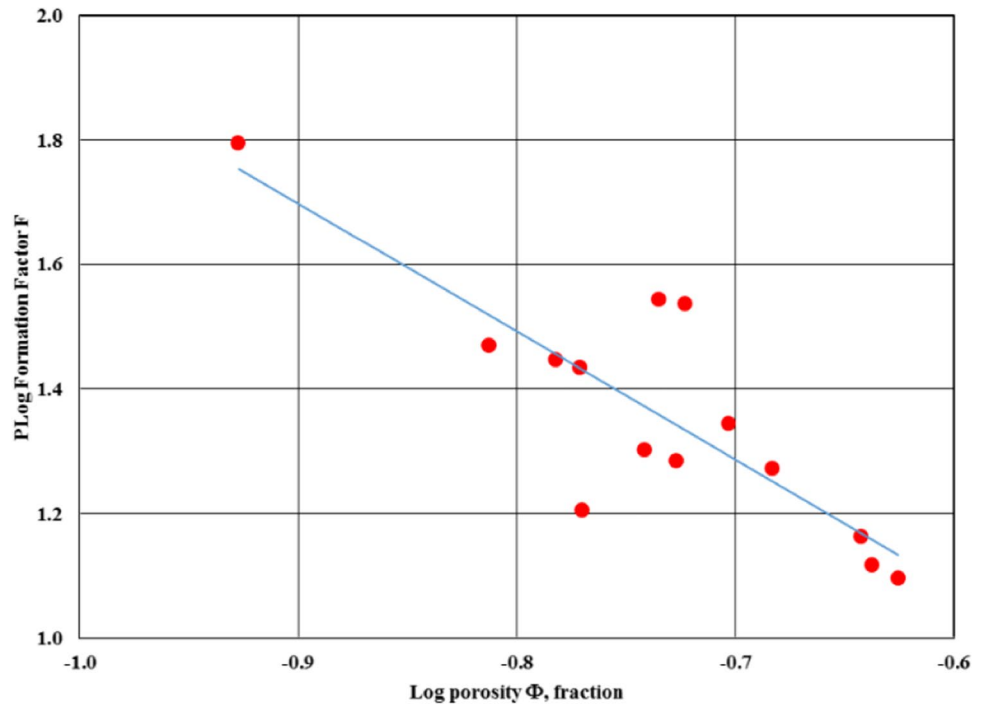
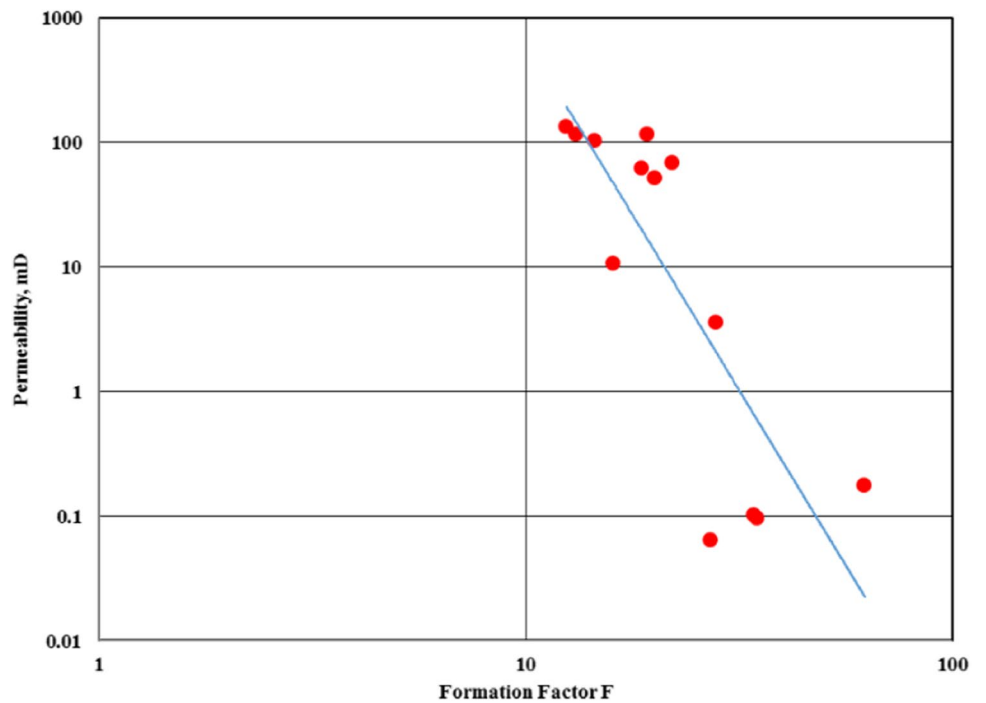


**Fig. 12** Permeability versus formation factor for Upper Cretaceous sandstone samples



**Longitudinal and transversal relaxation time comparison**

As shown in Figs. 14 and 15, samples of higher porosity and permeability have longer relaxation times, and a very close linear relationship is observed between the  $T_1$  and  $T_{2(100)}$  mean relaxation times with a determination coefficient  $R^2=0.96$  and controlled by the following equation:

$$T_{2(100)} = 0.58 T_1 \tag{16}$$

$T_{2(100)}$  is the NMR transversal relaxation time at 100 s. On the other hand, a nearly linear relationship is observed between the  $T_1$  and  $T_{2(600)}$  mean relaxation times

**Fig. 13** Permeability versus specific internal surface ( $S_{por}$ ) for Upper Cretaceous sandstone samples

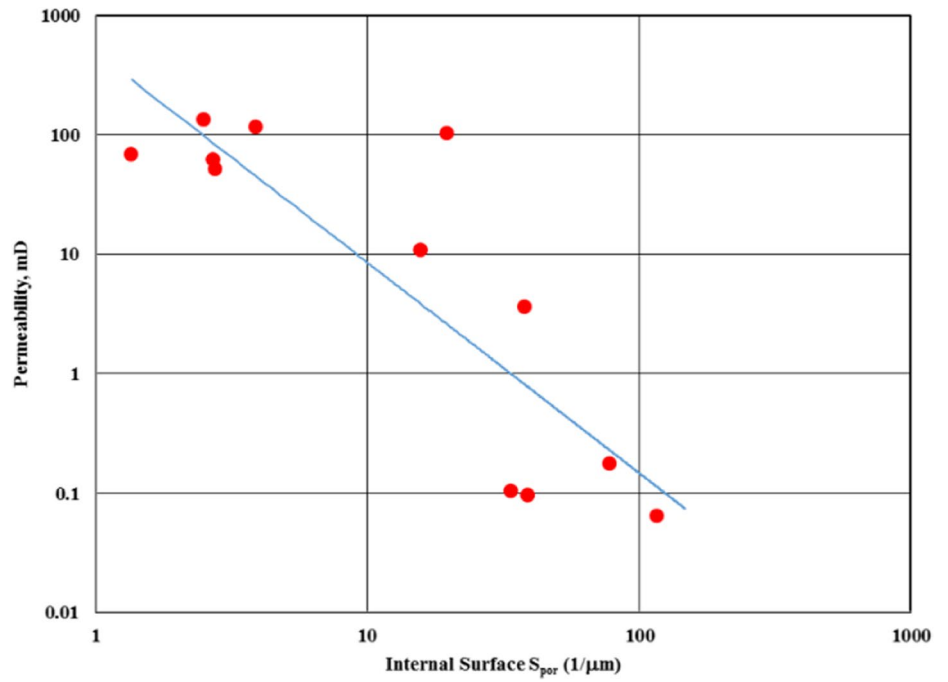
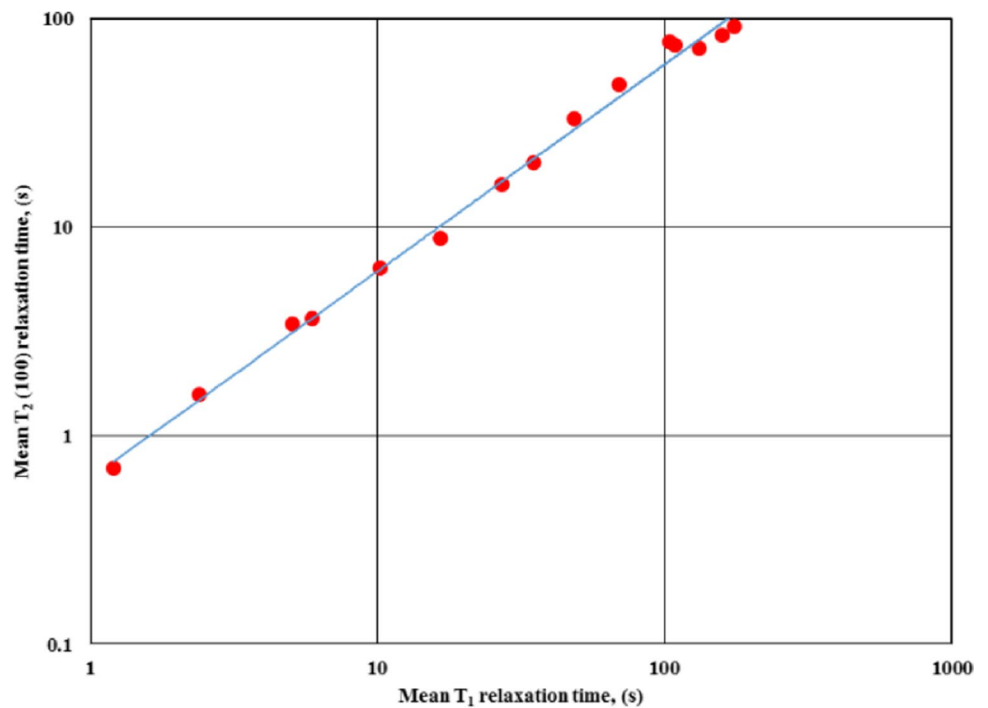


**Fig. 14** Mean relaxation time  $T_{2(100)}$  versus mean relaxation time  $T_1$  derived from NMR for Upper Cretaceous sandstone samples



with a coefficient of determination  $R^2=0.95$  and controlled by the following equation:

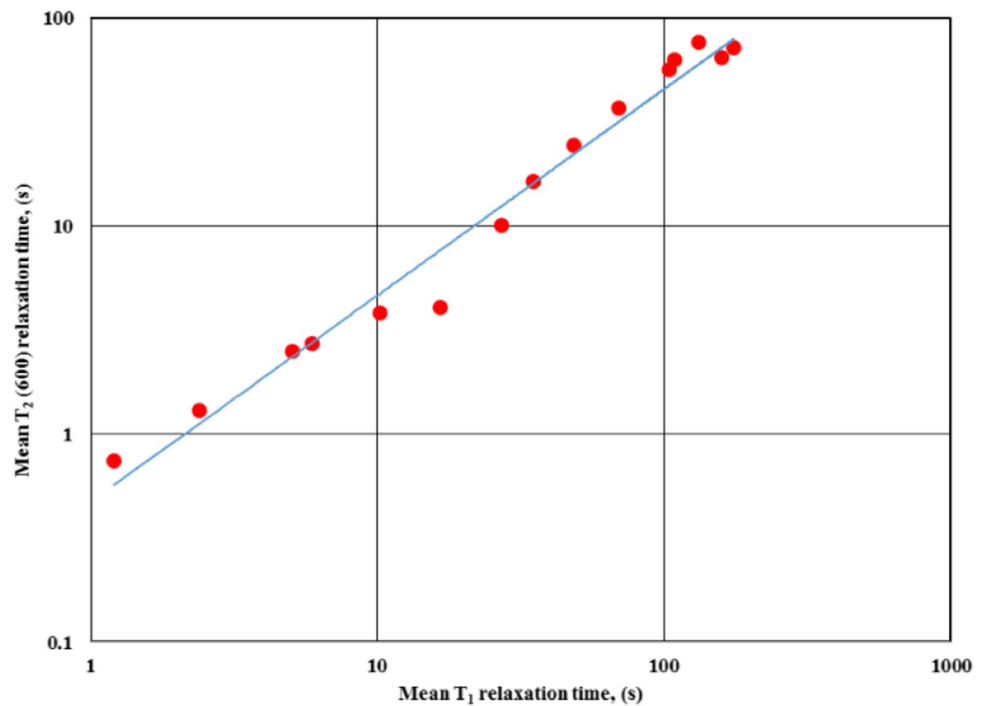
$$T_{2(600)} = 0.47 T_1 \tag{17}$$

$T_{2(600)}$  is the NMR transversal relaxation time at 600 s.

Assuming that the pore size distribution estimation based on the two mean relaxation times in the investigated

sandstones in a similar way is valid, the  $T_1/T_{2(100)}$  ratio is slightly higher for samples  $T_{2(100)}/T_1= 0.58$  in comparison with  $T_{2(600)}/T_1= 0.47$ . The observed differences in the ratio  $T_1/T_2$  can be caused by the ferromagnetic contribution of the Fe-chlorite that causes faster decay of transversal relaxation and stronger inhomogeneity in the magnetic field (Abuseda et al. 2016) which agrees with the observations in Keating and Knight (2007) performed on iron oxide-coated sands.

**Fig. 15** Mean relaxation time  $T_{2(600)}$  versus mean relaxation time  $T_1$  derived from NMR for Upper Cretaceous sandstone samples



### Petrophysical model for permeability prediction

A petrophysical model is usually made to predict a necessary reservoir parameter that is hard to measure. The model should be created to conclude this parameter from an easily measurable other physical parameters. Many theoretical models are applied for estimating the permeability using other petrophysical reservoir parameters.

### Permeability prediction

We compared the permeability prediction models used for the Upper Cretaceous sandstone samples to evaluate the model predictive power, and also the root means square (*rms*) deviation between the measured permeability (*k*) and predicted permeability (*k\**) is determined:

$$rms = \sqrt{\frac{1}{n} \sum_{i=1}^n (\log_{10}k - \log_{10}k_i^*)^2} \tag{18}$$

where *n* is the number of samples.

The average deviation between calculated and measured permeability is given by

$$d = \frac{1}{n} \sum_{i=1}^n |\log_{10}(k) - \log_{10}(k_i^*)| \tag{19}$$

A value of *d* = 1 indicates an average absolute deviation of one order of magnitude, in other words, a factor of 10.

### Permeability prediction using spectral induced polarization

Figure 12 shows the strong relation between permeability and formation factor, where the equation that determines the predicted permeability is as follows:

$$k = a * [F]^b \tag{20}$$

where *a* and *b* values are resulted from the relation itself. The predictive quality of equation (20) with *b* = -5.62 resulting in *rms* = 0.746 and *d* = 0.626. Figure 16 shows good agreement between the measured and predicted permeability for the majority of samples. Table 1 shows the resulting factors (*a* and *R*<sup>2</sup>) and the values of *rms* and *d*.

The previous research used the parameters derived from spectral induced polarization (SIP) as inputs in different permeability prediction models (e.g., Börner et al. 1996; Weller et al. 2010a). A general model is used here to integrate the formation factor and conductivity imaginary part ( $\sigma''$ ) measured at 1 Hz frequency for the fully saturated samples with a 100 mS/m fluid conductivity. Equation (21) was used to predict permeability:

$$k_{SIP}^* = aF^b(\sigma'')^c \tag{21}$$

where multiple regression has been used to determine *a*, *b*, and *c*. Equation (22) considers the conductivity imaginary part

$$k^* = 10^7 * 5.276 * F^{-6.055}(\sigma'')^{-1.423} \tag{22}$$

**Fig. 16** Comparison of measured and predicted permeability using formation factor for the Upper Cretaceous sandstone samples. The two dashed lines on either side of the diagonal indicate a deviation of one order of magnitude from the measured permeability value

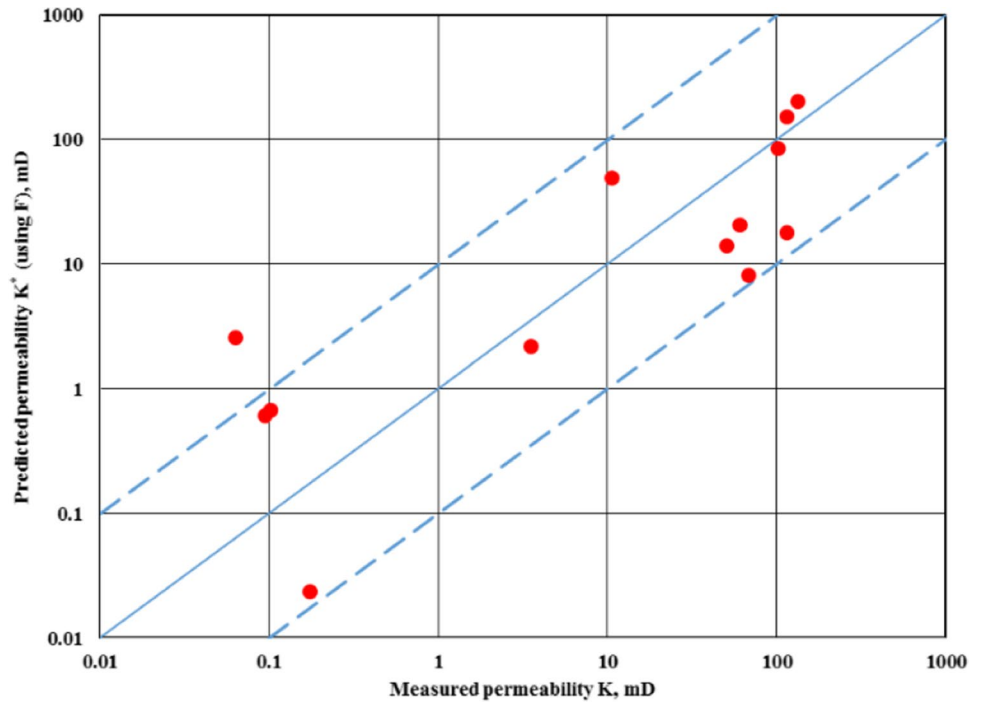


**Table 1** Comparison between measured permeability (*k*) and predicted permeability (*k\**)

No.	Equation	<i>a</i>	<i>R</i> <sup>2</sup>	<i>rms</i>	<i>d</i>
1	$k^* = [F]^{-5.62}$ Eq. (14)	$10^{8.46}$	0.68	0.75	0.63
2	$k^* = F^{-6.055}(\sigma'')^{-1.423}$ Eq. (22)	$5.276 \times 10^7$	0.75	0.65	0.53
3	$k^* = S_{por}^{-1.76}$ Eq. (15)	$10^{2.69}$	0.73	0.69	0.54
4	$k^* = F^{-3.144} * (S_{por})^{-1.116}$ Eq. (24)	$1.751 \times 10^6$	0.85	0.50	0.39
5	$K^* = a_1 T_1^2 \Phi^4$ Eq. (25)	4.16	0.84	0.55	0.46
6	$K^* = a_2 T_{2(100)}^2 \Phi^4$ Eq. (25)	11.30	0.86	0.51	0.44
7	$K^* = a_2 T_{2(600)}^2 \Phi^4$ Eq. (25)	20.76	0.90	0.44	0.39
8	$K^* = a T_1^{1.601} * F^{-2.251}$ Eq. (26)	23.791	0.91	0.40	0.30
9	$K^* = a T_{2(600)}^{1.799} * F^{-1.318}$ Eq. (27)	2.688	0.95	0.29	0.23

where *k\** is in mD and  $\sigma''$  in mS/m. Figure 17 shows a good agreement between the measured and predicted permeability in most samples, while Table 1 summarizes the factors and *rms* and *d* values. The deviation between the measured and predicted permeability is shown with the two dashed lines to both sides of the diagonal. Only one sample shows deviation more than one order of magnitude. The prediction quality will slightly improve by integrating the conductivity imaginary part.

**Permeability prediction using specific internal surface (*S<sub>por</sub>*)**

Figure 13 shows excellent correlation between permeability and *S<sub>por</sub>*; the following equation predicts the permeability using *S<sub>por</sub>*:

$$k = a * S_{por}^b \tag{23}$$

The relation between internal surface (*S<sub>por</sub>*) and permeability is used to determine the factor *a* and the exponents *b*, with prediction quality calculated using Eq. (23) of *b* = -1.76 resulting in *rms* = 0.688 and *d* = 0.539. Figure 18 shows a good agreement between the measured and predicted permeability for the majority of samples, and Table 1 summarizes the factors and *rms* and *d* values.

Replacing the porosity with the specific internal surface (*S<sub>por</sub>*) will improve the permeability prediction for our set samples. Equation 15 is a considerably higher coefficient of determination than Eqs. 9 and 14, and multiple regression is used to determine the exponents of the power law. The equation of permeability prediction using the internal surface and formation factor (*F*) reads is as follow:

$$k^* = 10^6 * 1.751 * F^{-3.144} * (S_{por})^{-1.116} \tag{24}$$

with *S<sub>por</sub>* in 1/μm., *k\** in mD, and *F* as unitless. Figure 19 shows that the *rms* and *d* confirms the excellent predictive quality for specific internal surface (*S<sub>por</sub>*) based on the measured permeability and the predicted permeability using Eq. (24). The factors and the *rms* and *d* values are in Table 1.

**Fig. 17** Comparison of measured and predicted permeability using electrical quantities for the Upper Cretaceous sandstone samples. The two dashed lines on either side of the diagonal indicate a deviation of one order of magnitude from the measured permeability value

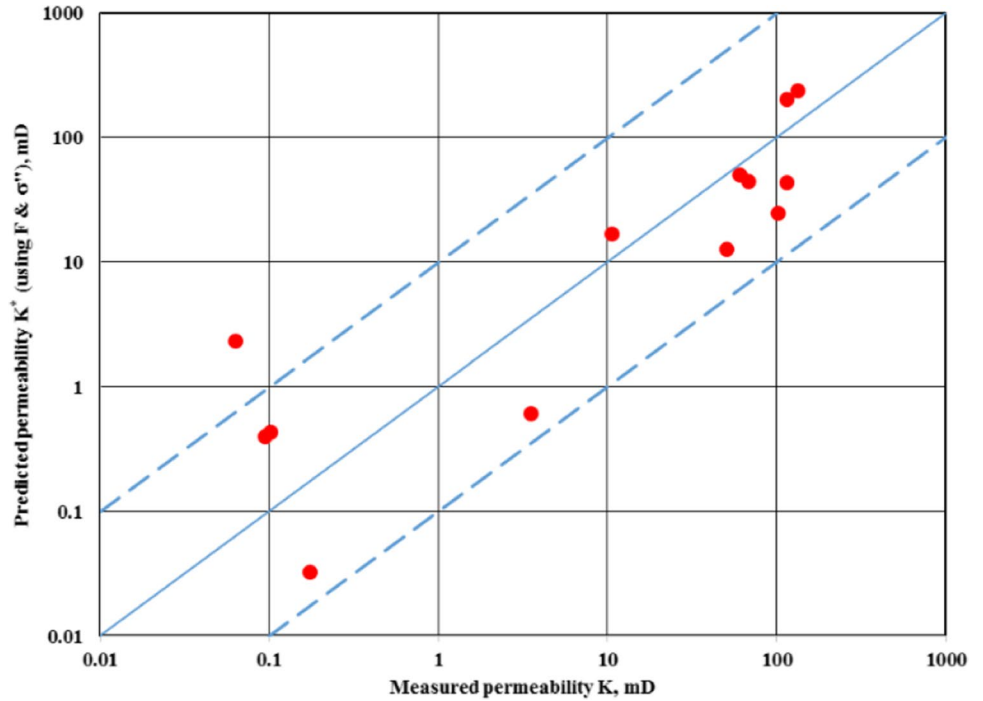
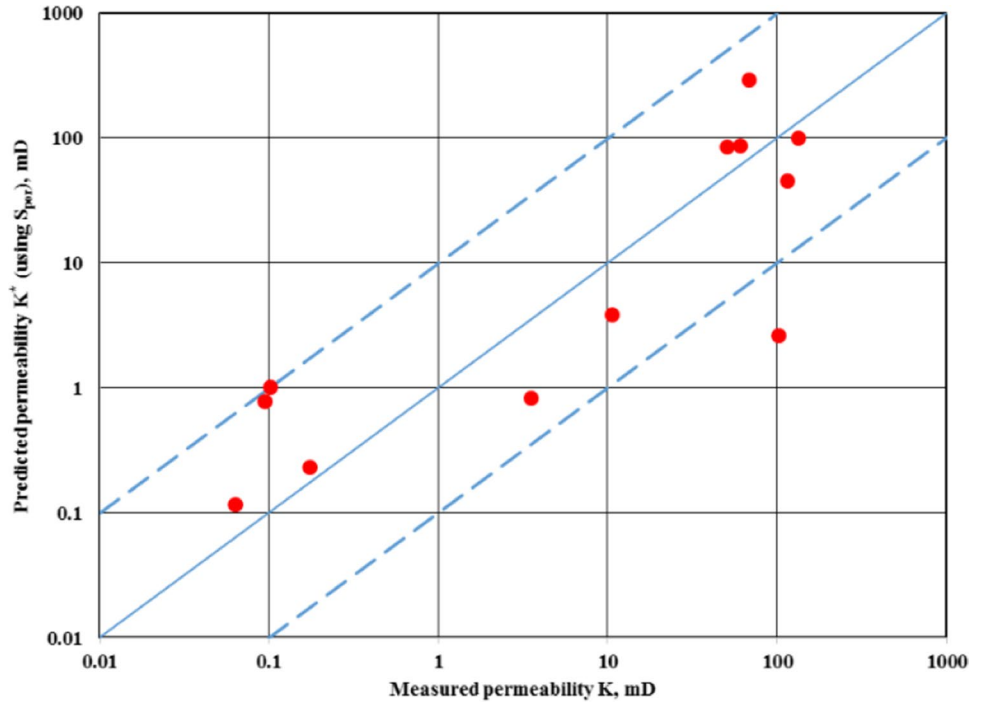


**Fig. 18** Comparison of measured and predicted permeability using internal surface ( $S_{por}$ ) for the Upper Cretaceous sandstone samples. The two dashed lines on either side of the diagonal indicate a deviation of one order of magnitude from the measured permeability value



**Permeability prediction from NMR**

The Kenyon empirical equation (Kenyon 1997) is commonly used for permeability estimation using the porosity and mean relaxation time

$$k_{NMR}^* = a_{1,2} T_{1,2}^2 \Phi^4 \tag{25}$$

The factors  $a_{1,2}$  depend on the corresponding relaxation times of  $T_1$  or  $T_2$ . The exponent of 2 for the relaxation time is based on the proportionality consideration between the pore

**Fig. 19** Comparison of measured and predicted permeability using formation factor and specific internal surface ( $S_{por}$ ) for the Upper Cretaceous sandstone samples. The two dashed lines on either side of the diagonal indicate a deviation of one order of magnitude from the measured permeability value

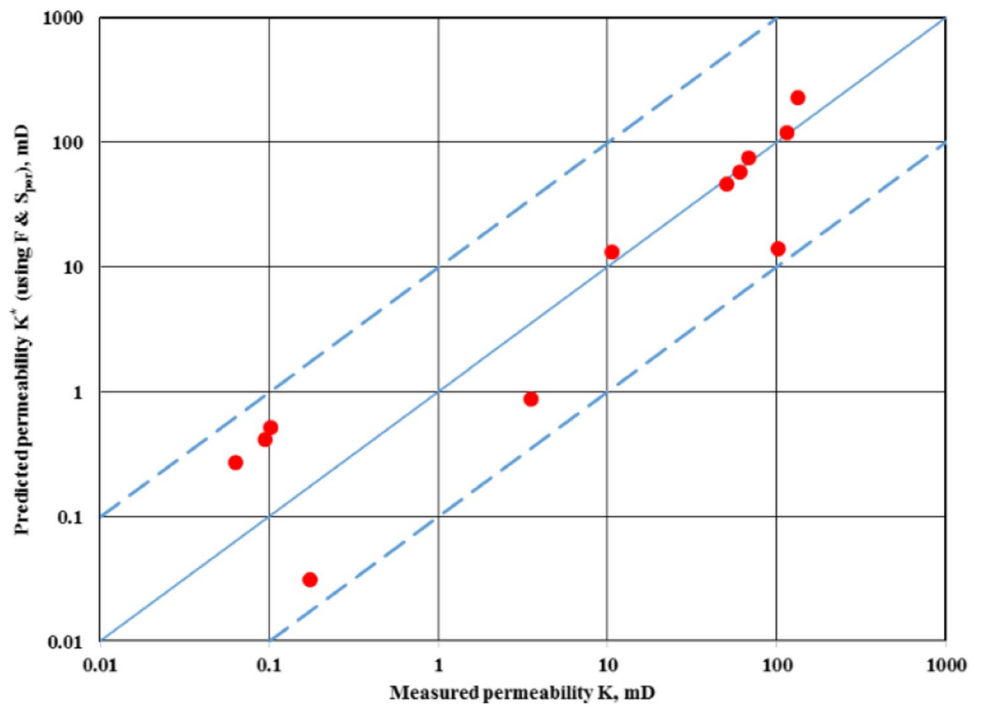
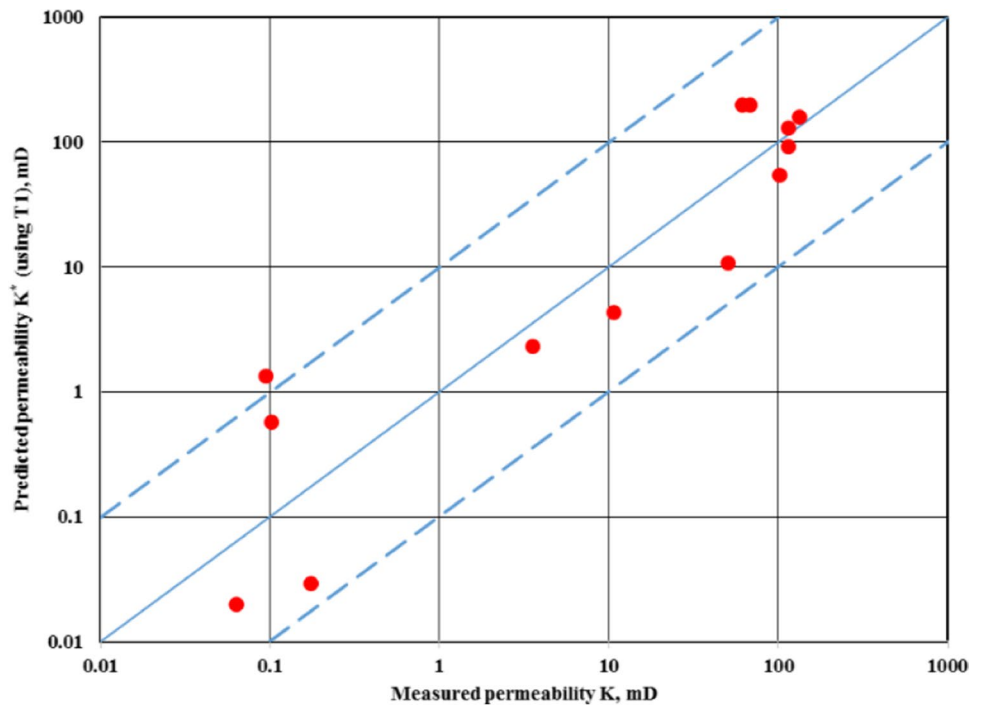


**Fig. 20** Comparison of measured and predicted permeability using longitudinal relaxation time ( $T_1$ ) and porosity for the Upper Cretaceous sandstone samples. The two dashed lines on either side of the diagonal indicate a deviation of one order of magnitude from the measured permeability value



radius  $r$  and relaxation time in Eq. (7). The porosity exponent was previously determined in empirical studies (Coates et al. 1999; Dunn et al. 2002). Equation (25) is used for predicting the permeability by inputting the porosity, mean longitudinal relaxation time  $T_1$ , and the mean transversal relaxation time  $T_2$ . The factors  $a_1$  and  $a_2$  were determined by minimizing the root mean square ( $rms$ ) and average deviation ( $d$ ) between the

measured and predicted permeability, as shown in Figs. 20, 21, and 22, and also by replacing the porosity with the formation factor. The resulting equation will be as follows:

$$K^* = 23.791 * T_1^{1.601} * F^{-2.251} \tag{26}$$



**Fig. 21** Comparison of measured and predicted permeability using transversal relaxation time ( $T_{2(100)}$ ) and porosity for the Upper Cretaceous sandstone samples. The two dashed lines on either side of the diagonal indicate a deviation of one order of magnitude from the measured permeability value

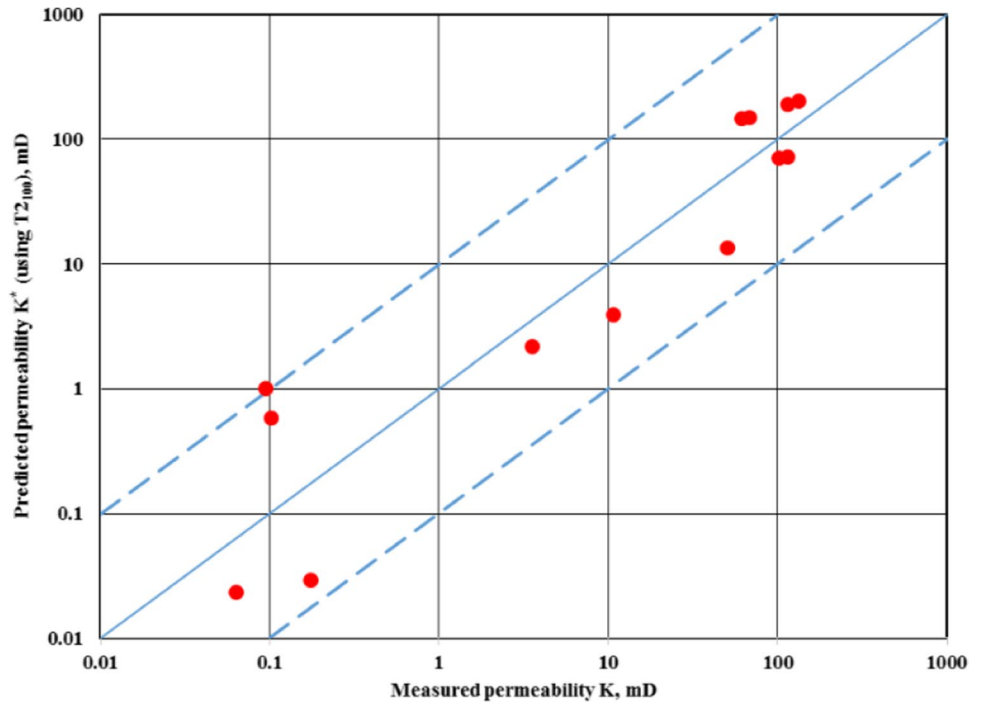
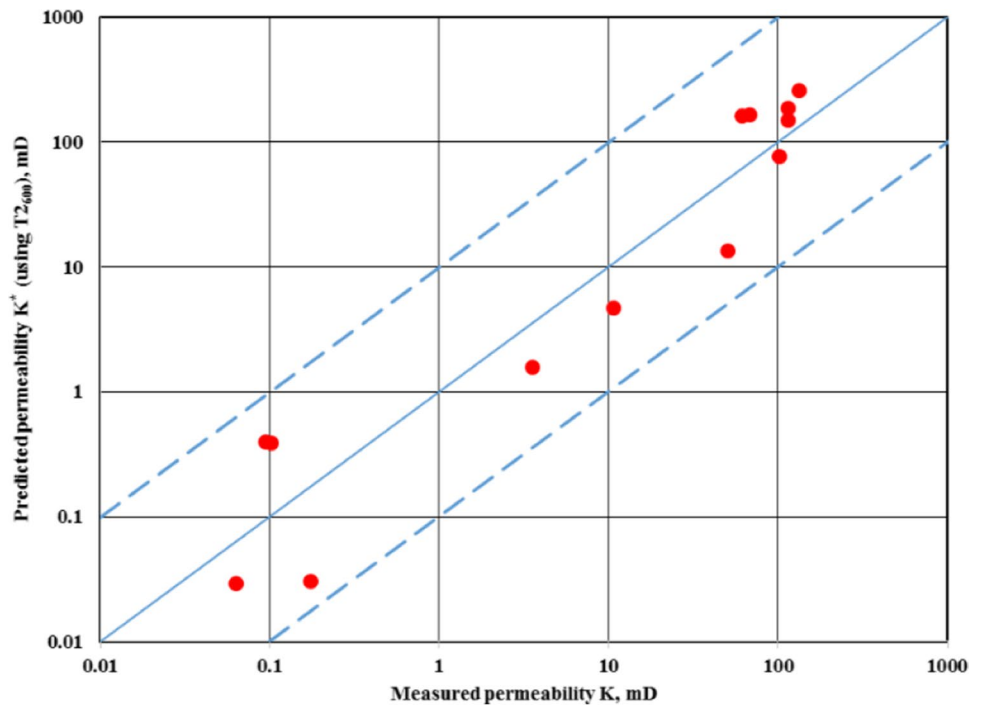


**Fig. 22** Comparison of measured and predicted permeability using transversal relaxation time ( $T_{2(600)}$ ) and porosity for the Upper Cretaceous sandstone samples. The two dashed lines on either side of the diagonal indicate a deviation of one order of magnitude from the measured permeability value



$$K^* = 2.688 * T_{2(600)}^{1.799} * F^{-1.318} \tag{27}$$

with  $T_1$  and  $T_2$  in sec. and  $k^*$  in mD and  $F$  as unitless.

**Fig. 23** Comparison of measured and predicted permeability using the longitudinal relaxation time ( $T_1$ ) and formation factor for the Upper Cretaceous sandstone samples. The two dashed lines on either side of the diagonal indicate a deviation of one order of magnitude from the measured permeability value

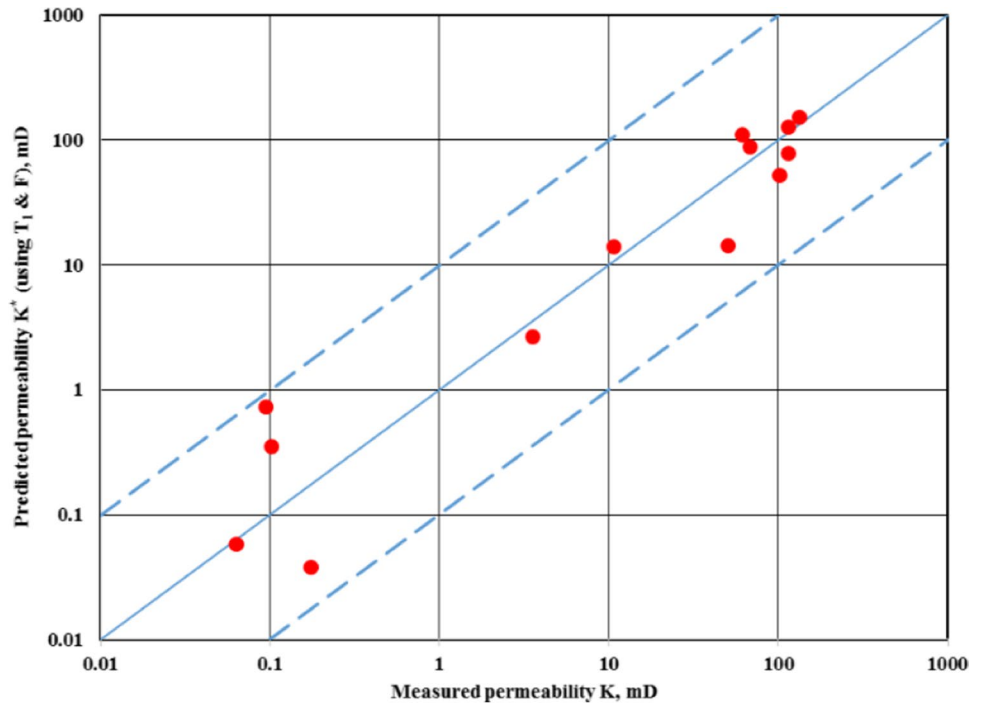
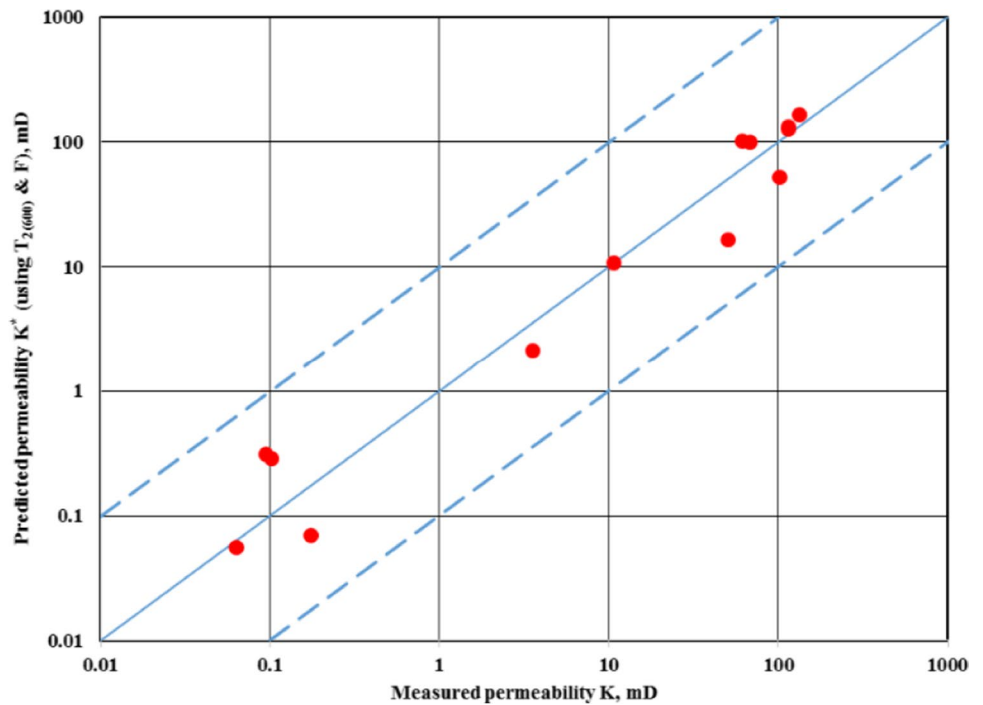


**Fig. 24** Comparison of measured and predicted permeability using the transversal relaxation time ( $T_{2(600)}$ ) and formation factor for the Upper Cretaceous sandstone samples. The two dashed lines on either side of the diagonal indicate a deviation of one order of magnitude from the measured permeability value



Figures 23 and 24 show excellent prediction quality between the measured permeability and the permeability prediction using Eqs. (26) and (27), respectively, and the values of  $rms$  and  $d$  are summarized in Table 1.

### Summary

An investigation has been done for the relations between different petrophysical parameters of the Upper Cretaceous Bahariya Formation. The high values of porosity and the permeability occur mainly in quartz arenite which

characterized by coarse to medium grains with the absence of detrital materials, while the low values of porosity and the permeability occur in quartz wackes which are fine grains, silty sizes, and clays. Significant correlations between a variety of parameters to porosity and/or permeability have been proven. Permeability prediction based on porosity is not as accurate as using the formation factor because of the large scattering in the relevant cross plot. Also considering the superiority of the formation factor in ability of describing the connected pore space effectively, a better understanding of the formation evaluation was provided by the cross-plot between RQI and FZI; it typically has  $0.02 \mu\text{m} < \text{RQI} \leq 0.78 \mu\text{m}$  indicating impermeous to fair reservoir quality. Estimated ( $R_{35}$ ) range is (0.10–7.40  $\mu\text{m}$ ). The Upper Cretaceous sandstone reservoir is comprised of meso-microporosity ( $0.10 \mu\text{m} < R_{35} \leq 2 \mu\text{m}$ ) and macro-porosity ( $2 \mu\text{m} < R_{35} \leq 10 \mu\text{m}$ ). Based on core-based reservoir characterization, the macro-porosity of the Upper Cretaceous sandstone have the fair reservoir quality and hydraulic flow units ( $0.09 \mu\text{m} < \text{FZI} \leq 3.39 \mu\text{m}$ );  $\text{RQI} < (1 \mu\text{m})$ . The cross-plot between the log values of porosity and formation factor is an expected trend, i.e., decreasing formation factor with increasing porosity, and gives a cementation factor  $m = 1.85$  which results in a high coefficient of determination ( $R^2 = 0.70$ ). Our study confirms the importance of the formation factor in predicting the permeability of Upper Cretaceous sandstone samples. The conductivity imaginary part is proved to be with less importance. The specific internal surface has more importance for permeability prediction than the porosity and formation factor. The NMR relaxation times and porosity models have been proven to be more adequate and accurate for permeability prediction. Replacing the porosity with the formation improves the permeability prediction. Multiple regression should be used to determine the exponents of the power law equation, and a slightly better permeability prediction is achieved by using the transversal relaxation time  $T_{2(600)}$ .

**Funding** Open access funding provided by The Science, Technology & Innovation Funding Authority (STDF) in cooperation with The Egyptian Knowledge Bank (EKB).

## Declarations

**Conflict of interest** The authors declare that they have no competing interests.

**Open Access** This article is licensed under a Creative Commons Attribution 4.0 International License, which permits use, sharing, adaptation, distribution and reproduction in any medium or format, as long as you give appropriate credit to the original author(s) and the source, provide a link to the Creative Commons licence, and indicate if changes were made. The images or other third party material in this article are included in the article's Creative Commons licence, unless indicated otherwise in a credit line to the material. If material is not included in

the article's Creative Commons licence and your intended use is not permitted by statutory regulation or exceeds the permitted use, you will need to obtain permission directly from the copyright holder. To view a copy of this licence, visit <http://creativecommons.org/licenses/by/4.0/>.

## References

- Abuseda H, El Sayed AMA (2022) Petrographical and petrophysical studies of some Upper Cretaceous rocks, Western Desert, Egypt. *JJEES* 13(1):37–47
- Abuseda H, Weller A, Sattler C-D, Debschütz W (2016) Petrographical and petrophysical investigations of upper cretaceous sandstones of the South West Sennan field, Western Desert, Egypt. *Arab J Geosci* 9:212. <https://doi.org/10.1007/s12517-015-2156-1>
- Adler PM, Jaacquin CG, Quibier JA (1990) Flow in simulated porous media. *Inter. J. Multiphase flow* 16:691–712
- Al-Ghuribawi MM, Faisal RF (2021) An integrated microfacies and well logs-based reservoir characterization of Yamama Formation, Southern Iraq. *Iraqi J. Sci.* 62(10):3570–3586. <https://doi.org/10.24996/ij.s.2021.62.10.16>
- Amaefule JO, Altunbay M, Tiab D, Kersey DG, Keelan DK (1993) Enhanced reservoir description: using core and log data to identify hydraulic (flow) units and predict permeability in uncored intervals/wells. In: SPE annual technical conference and exhibition. Society of Petroleum Engineers
- Börner FD, Schopper JR, Weller A (1996) Evaluation of transport and storage properties in the soil and groundwater zone from induced polarization measurements. *Geophys. Prospect.* 44:583–601
- Brunauer S, Emmett PH, Teller E (1938) Adsorption of gases in multimolecular layers. *J. Am. Chem. Soc.* 60:309–319
- Carman PC (1937) Fluid flow through granular beds. *Trans Inst. Chem. Eng.* 15:150–166
- Catuneanu O, Khalifa MA, Wanas HA (2006) Sequence stratigraphy of the Lower Cenomanian Bahariya Formation, Bahariya Oasis, Western Desert, Egypt. *Sediment. Geol.* 190:121–137
- Coates GR, Xiao LZ, Prammer MG (1999) NMR logging principles and applications. Halliburton Energy Services, Houston
- Dodge WS, Shafer JL, Guzman-Garcia AG, Noble DA (1995) Core and log NMR measurements of an iron-rich, glauconitic sandstone reservoir. 36th Annual Symposium of SPWLA, Paris, France
- Dominik W (1985) Stratigraphie und Sedimentologie der Oberkreide von Bahariya und ihre Korelation zum Dakhla Becken (Western Desert Agypten). *Berlin Geowiss. Abh.* 50:153–176
- Dunn K-J, Bergman DJ, LaTorraca GA (2002) Nuclear magnetic resonance. Petrophysical and logging applications. In: Handbook of Geophysical Exploration. Seismic Exploration, vol 32. Pergamon
- El Gezeery, N.H., Mohsen, S.M., Farid, M.I. (1972). "Sedimentary basins of Egypt and their petroleum prospects." 8th Arab Pet. Cong., Algiers, Paper No. 83 (B-3), 13 p.
- El Sayed AMA et al (1998) Poisson's ratio and fluid saturation: Upper Cretaceous, Egypt, vol 98. *Min Chem, Siófok, Hungary*
- El Sayed AMA (2011) Thermophysical study of sandstone reservoir rocks. *J. Pet. Sci. Eng.* 76(3-4):138–147
- El Sayed AMA et al (2019) IOP Conf. Ser.: Earth Environ. Sci 221:012047
- Farouk S, Sen S, Ganguli SS, Abuseda H, Debnath A (2021) Petrophysical assessment and permeability modeling utilizing core data and machine learning approaches – a study from the Badr El Din-1 field, Egypt. *Mar. Pet. Geol.* 133:105265. <https://doi.org/10.1016/j.marpetgeo.2021.105265>
- Farouk S, Sen S, Abuseda H, El-Shamly Y, Salam A, Elhossainy MM (2022) Petrophysical characterization of the Turonian and

- Cenomanian intervals in the Abu Gharadig field, Western Desert, Egypt: Inferences on Reservoir Quality and Resource Development. *Nat. Resour. Res.* 31(3):1793–1824
- Franks GD (1982) Stratigraphical modeling of Upper Cretaceous sediments of Bahariya Oasis, 6th edn. EGPC Exp. Seminar, Cairo, p 21
- Glover P, Zadjali I, Frew K (2006) Permeability prediction from MICP and NMR data using an electrokinetic approach. *Geophysics* 71:49–60
- Harishidayat D, Farouk S, Abioui M, Aziz OA (2022) Subsurface fluid flow feature as hydrocarbon indicator in the Alamein Basin, Onshore Egypt; Seismic Attribute Perspective. *Energies* 15(9):3048
- Herron MM (1987) Estimating of intrinsic permeability of elastic sediments from geochemical data. *Trans., SPWLA*, p 6
- Hidajat I, Singh M, Cooper J, Mohanty KK (2002) Permeability of porous media from simulated NMR response. *Transp Porous Media* 48:225–247
- Kassab MA, Teama MA (2018) Hydraulic flow unit and facies analysis integrated study for reservoir characterization: a case study of Middle Jurassic rocks at Khashm El-Galala, Gulf of Suez, Egypt. *Arabian J. of Geoscience*, Springer 11(12):294. <https://doi.org/10.1007/s12517-018-3595-2>
- Keating K, Knight R (2007) A laboratory study to determine the effect of iron oxides on proton NMR measurements. *Geophysics* 72(1):E27–E32
- Kenyon WE (1992) Nuclear magnetic resonance as a petrophysical measurement. *Nuclear Geophysics* 6(2):153–171 Later revised and published in 1997 as *Petrophysical principles of applications of NMR logging*, *The Log Analyst*, v. 38, no. 2, p. 21–43
- Kenyon WE (1997) *Petrophysical principles of applications of NMR logging*. *The Log Analysts* 38(2):21–43
- Kolodzie, Jr. (1980). Analysis of pore throat size and use of the Waxman-Smits equation to determine OOIP in Spindle field, Colorado: Society of Petroleum Engineers 55th Annual Fall Technical Conference, SPE Paper 9382, 10
- Lala A, El Sayed N (2017) Controls of pore throat radius distribution on permeability. *J. Pet. Sci. Eng.* 157(2017):941–950
- Lesmes DP, Morgan FD (2001) Dielectric spectroscopy of sedimentary rocks. *J Geophys Res* 106:13329–13346
- Marshall DJ, Madden TR (1959) Induced polarization, a study of its causes. *Geophysics* 24:790–816
- Matthias HA, Weller A, Sattler C-D, Debschütz W, El-Sayed AMA (2009) A complex core-log case study of an anisotropic sandstone, originating from Bahariya Formation, Abu Gharadig Basin, Egypt. *Petrophysics* 50(6):478–497
- Revil A, Florsch N (2010) Determination of permeability from spectral induced polarization in granular media. *Geophys J Int* 181(3):1480–1498
- Scheidegger AE (1974) *The physics of flow through porous media*. University of Toronto, Toronto Press, p 353
- Schön JH (1996) *Handbook of Geophysical Exploration: Fundamentals and Principles of Petrophysics*. In: *Seismic Exploration. Physical Properties of Rocks*. Pergamon
- Shalaby A, Sarhan MA (2021) Origin of two different deformation styles via active folding mechanisms of inverted Abu El Gharadig Basin, Western Desert, Egypt. *J. African Earth Sci.* 183:104331
- Soliman, S. M., Faris, El-Badry, O. (1970). Lithostratigraphy of the Cretaceous formations of the Bahariya Oasis, Western Desert, Egypt 7th Arab Pet. Cong., 59, (B-3), 30, Kuwait
- Tiab D, Donaldson EC (2015) *Petrophysics: theory and practice of measuring reservoir rock and fluid transport properties*. Gulf professional publishing
- Timur A (1968) An investigation of permeability, porosity, and residual water saturation relationships. In: 9th Ann. Logging Symp. SPWLA, pp 1–18
- Titov K, Tarasov A, Ilyn Y, Seleznev N, Boyd A (2002) Relationships between induced polarization relaxation time and hydraulic properties of sandstone. *Geophys J. Int* 180:1095–1106
- Weller A, Nordsiek S, Debschütz W (2010a) Estimating permeability of sandstone samples by nuclear magnetic resonance and spectral-induced polarization. *Geophysics* 75(6):E 215–EE226. <https://doi.org/10.1190/1.3507304>
- Weller A, Slater L, Nordsiek S, Ntarlagiannis D (2010b) On the estimation of specific surface per unit pore volume from induced polarization: a robust empirical relation fits multiple data sets. *Geophysics* 75(4):WA105–WA112. <https://doi.org/10.1190/1.3471577>
- Lala A, El Sayed N (2015) Calculating absolute permeability using nuclear magnetic resonance models. *Arab J Geosci*. <https://doi.org/10.1007/s12517-015-1841-4>